

## Optimization of the Stirring Parameters of AZ91Mg-based Stir Casted Hybrid Composites using Taguchi and ANN

Kamal Kant Singh\* & Dharamvir Mangal

Gautam Buddha University, Greater Noida 201 312, Utter Pradesh, India

Received 24 January 2022; revised 26 February 2023; accepted 07 March 2023

In the current research, the fabricated Mg hybrid composites amalgamate with the vacuum-based squeezed stir casting process having TiC and Al<sub>2</sub>O<sub>3</sub> reinforcement's in which AZ91Mg-alloy is the base material. The study includes the processing parameters of the vacuum-based squeezed stir casting method (such as stirring time, stirrer depth, and stirring speed) that have been varied and then investigates their influential effect by using the L<sub>16</sub> orthogonal Taguchi approach. By considering these parameters, the tribo-mechanical properties are also optimized like porosity, ultimate strength, and rate of wear loss of Mg-hybrid composites. The result reveals a significant association between processing parameters and optimized tribo-mechanical properties. The results signify that the processing parameters are best optimized at processing parameters of 500 rpm of stirring speed, 5 min of stirring time, and 50 mm of stirrer depth and the optimized tribo-mechanical properties are 0.4% porosity, 245 MPa of ultimate strength, and 0.0011 mm<sup>3</sup> per min is the loss of wear rate. However, the ANOVA results contribute that the stirrer depth has the most significant processing parameter compared to other optimized parameters. This research also includes an artificially designed networking model which validates the designated set of empirical data. Thus due to their suitability for abrasion wear AZ91-hybrid composite gives a new divergence towards the designing parts of minuscule airplanes used in surveillance applications such as ailerons and wing flaps.

**Keywords:** Artificial neural network, Mg-Hybrid composites, Stirrer optimize, VSSC technique, Taguchi approach

### Introduction

Nowadays, during fabrication casting, surface deformities such as gas holes, white inclusions have been observed in Mg/Al matrix composites which minimize the potential ability of hard reinforcements in the fabricated composites. These defects also depreciate the strengthening properties of fabricated composites.<sup>1,2</sup> Therefore, the better alternative for this problem is the use of hybrid composite materials because their mechanical and tribological properties are customized as per the requirements.<sup>3</sup> The most frequently counted reinforcing materials in Mg-matrix are reviewed as boron carbide, silicon carbide, silicon nitride alumina, and TiC, etc.<sup>4</sup>

The stir casting method is a commonly used fabrication technique to fabricate Al/Mg matrix composites. This method provides homogeneous distribution in Al/Mg matrix composites with the least defects as compared to other processing techniques.<sup>5-7</sup> Singh and Chauhan compared the mechanical properties of Mg/B<sub>4</sub>C composites using electromagnetic and squeezed-pressure stir casting processes.<sup>8</sup> Their study

reveals that Mg-composites fabricated by squeezed stir-casting technique shows improved mechanical results as compared to the electromagnetic stir-casting technique with the least defects. Singh *et al.*<sup>9</sup> fabricate Mg/B<sub>4</sub>C hybrid composites by employing the same fabrication method and using the statistical Taguchi approach to evaluate the mechanical properties. Their study evaluates the improved hardness and tensile properties of Mg/B<sub>4</sub>C hybrid composites when compared with Mg-matrix base material. Muhammad *et al.*<sup>10</sup> studied Al-hybrid composites using a simulated statistical approach with the same fabrication technique and considering the parameters like stirring diameter and stirring speed. Their study accomplishes significant results without depreciating their microstructural properties. Then, another study performed by Deepak *et al.*<sup>11</sup> illustrated the homogeneous dispersion of aluminum oxide (up to 6 wt.%) in Mg-based composites and leads to minimal deformities by using the same stir-casting fabrication method.

In the literature study, researchers also propose different mathematical tools like neural networks and regression models.<sup>12-14</sup> These models design a suitable association of input-output values by using different mathematical tools. With the help of different multi-

\* Author for Correspondence  
E-mail: kamalkantsingh.kc@gmail.com

response optimization tools, input parameter values are identified. During fabrication, the processing parameters reflect the service conditions of the fabricated composite as input parameters. The output factors help to determine the actual turnout values without repeating experimental fabrication trial runs. However, the output factors are mechanical and tribological parameters of the fabricated composites like hardness, modulus of elasticity, friction coefficient, and wear rate.<sup>15–17</sup>

Aydin *et al.*<sup>18</sup> worked on regression analysis of fabricated Mg/TiC-based composites by the stir casting process. And their study investigated the influence of different parameters like applied load, reinforcement percentage, sliding speed, and distance. And based on these parameters, wear loss rate values of Mg/TiC-based composites have been evaluated and optimized results had been obtained. Jeyaprakasam *et al.*<sup>19</sup> evaluated the wear parameters of Al/TiC/Gr hybrid composites by using the surface method. According to their results, the sliding distance was the dominant factor that majorly affects the wear loss rate of Al-hybrid composites. Moreover, Prasad *et al.*<sup>20</sup> demonstrated the influence of TiC reinforcement with Mg/Si composites and examined the dry sliding wear conditions by using a Taguchi-based optimization method. Similarly, Samanta *et al.*<sup>21</sup> applied an orthogonal array approach to Mg-based composites and analyzed the significant optimized value of reinforcement (TiC) and their wear parameters. Rajmohan *et al.*<sup>22</sup> used the grey fuzzy (hybridized) method to forecast the optimal composition of wear rate and friction coefficient. Afzal *et al.*<sup>23</sup> demonstrate an artificial neural network design model as an effective approach to predicting the tribological behavior of Mg/Al<sub>2</sub>O<sub>3</sub> composites. Furthermore, Arif *et al.*<sup>24</sup> examined the wear loss of Al/SiC hybrid composites by employing the ANN model i.e. feed-forward back propagation method. Niranjana *et al.*<sup>25</sup> worked on optimizing the mechanical properties of Al-hybrid composites (alumina as reinforcing particles) by using the ANN model and considering processing temperature as one of the key parameters. Madhu *et al.*<sup>26</sup> determined the optimized wear parameters of Al/B<sub>4</sub>C/Gr composites by considering the processing parameters such as processing temperature and applied pressure by using artificial networking models. However, Anand *et al.*<sup>27</sup> designed the ANN model using non-linear regression parameters and illustrate the regression ANN model is more convenient than the basic ANN model design.

Thus, the above literature study stated that the Taguchi approaches and neural network models are conventionally discovered as the best-optimizing method for Mg-based composite materials but least work has been reported on Mg-hybrid composites using TiC and alumina as reinforcement fabricated through the Vacuum-Based Squeezed Stir Casting Method (VSSC).

Thus, the current study has been formulated by selecting two objectives by using VSSC processing (fabrication) parameters. The first objective is to examine the effect of stirring (fabrication) parameters of AZ91Mg hybrid composite by using the L<sub>16</sub> orthogonal Taguchi approach. Secondly objective is to formulate the tribo-mechanical properties (like porosity, ultimate strength, and loss of wear rate) of fabricated AZ91Mg-composites. Also, an ANN-based regression mathematical model is designed by using these parameters through this design; a limit of experimentation has been performed.

## Methodologies

### Material Selection

A Hybrid Mg-based composite has been fabricated using VSSC process. The optimized amounts of reinforcing particles were included in the hybrid Mg-composites which was previously evaluated in the literature.<sup>28</sup> The reinforcing particles, titanium carbide (98.5% purity, 150–300 microns), and aluminum oxide (99.9% purity, 100–300 microns) were procured from SAC (Sigma Aldrich Chemicals) Pvt. Ltd, Bangalore, and CDH (Chemical Drug House) Pvt. Ltd, Delhi respectively. Local vendors provide Mg-alloy ingot from India-mart Intermesh Ltd., Noida, UP, India having 98.9% purity. However, the illustration of the metallographic images of the matrix, reinforcements materials, and the fabricated composite has been represented in Fig. 1. The TiC and Al<sub>2</sub>O<sub>3</sub> reinforcements show irregular block and tubular shapes respectively, as shown in Fig. 1(a) and (b). Moreover, Fig. 1(c) presents the AZ91Mg alloy microscopic image having an erratic particle surface. The chemical distribution of AZ91Mg-alloy is 9.7 Al, 1.0 Zn, 0.5 Mn, 0.1Si, 0.005 Fe with a balance of pure Mg.

### Fabrication Method

The Mg-hybrid composites (85 wt.% AZ91, 9 wt.% TiC, and 6 wt.% Al<sub>2</sub>O<sub>3</sub>) are fabricated using squeezed vacuum-based stir casting method as shown in Fig. 2. Initially, to remove the moisture contents

from TiC and Al<sub>2</sub>O<sub>3</sub> reinforcing powders have been put in an electric oven at 300°C separately. Then under constant stirring, the AZ91 matrix (ingot) is placed in a vacuum-preheated furnace attached with Ar + SF<sub>6</sub> cover gas to control from the fire. Then TiC + Al<sub>2</sub>O<sub>3</sub> have been dropped into the AZ91 melt with constant stirring. About 800–850°C of stirring temperature and 455 rpm of stirring speed have been given to the fabricating setup to achieve uniform composition. Further, the stirring parameters set by the design of the experiment as mentioned in Table 1.

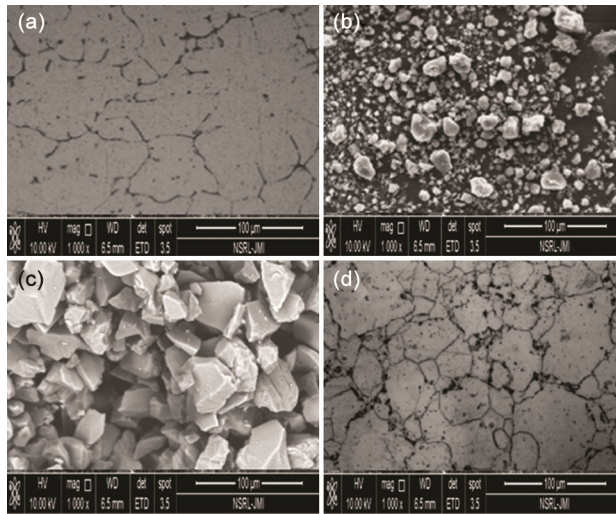


Fig. 1 — Microscopic images of (a) AZ91Mg-alloy, (b) Titanium carbide, (c) Alumina, and (d) AZ91/TiC/Al<sub>2</sub>O<sub>3</sub> hybrid composite

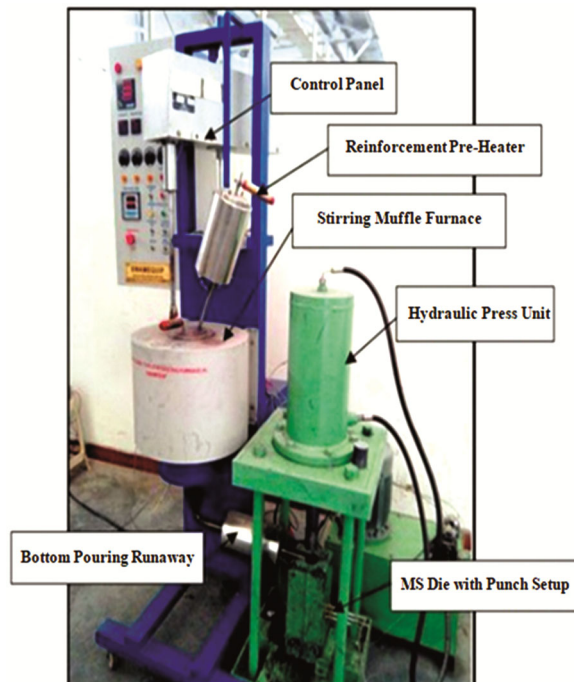


Fig. 2 — Vacuum-based squeezed stir casting setup

After 15 minutes of stirring, the hybridized melt has been dropped to the MS mold through the bottom pouring passage. It is a passage act as a pre-heater having a narrow inclined track (250°C) integrated at the bottom of the furnace to preserve the hybridized compo-melt. Then the compo-melt is released to the MS mold and immediately squeezed pressure (250 MPa) is provided by the hydraulic press for 10 minutes in order to eliminate the residual deformities. After solidification under atmospheric temperature, fabricated specimens moved out from MS mold and then cut out as per experimenting dimensions.

#### Orthogonal Taguchi Approach

According to Taguchi's orthogonal approach, the count of empirical trials has been calculated as 16 related to examining 3 factors at 4 distinct levels between the functioning ranges. The numbers of absolute variables for this experimental work are illustrated in Table 1 for 4 sets of levels. Each of the experiments was calculated according to the tabulated L<sub>16</sub> orthogonal array. The optimized results have been investigated as output responses as represent in Table 2.

Table 1 — Processing parameters and their levels

Factors	Factor Levels			
	1	2	3	4
A, Stirring Speed (rpm)	400	450	500	550
B, Stirring Time (min)	5	10	15	20
C, Stirring Depth (mm)	30	40	50	60

Table 2 — The experimental design matrix and their output result values

Sp No	A (rpm)	B (min)	C (mm)	P (%)	US (MPa)	WR (mm <sup>3</sup> /min)
S <sub>1</sub>	400	5	30	3.2	189	0.0077
S <sub>2</sub>	400	10	40	2.7	210	0.0062
S <sub>3</sub>	400	15	50	0.5	250	0.0021
S <sub>4</sub>	400	20	60	1.8	227	0.0039
S <sub>5</sub>	450	5	40	2.5	222	0.0050
S <sub>6</sub>	450	10	30	2.8	202	0.0070
S <sub>7</sub>	450	15	60	1.4	233	0.0031
S <sub>8</sub>	450	20	50	0.2	241	0.0013
S <sub>9</sub>	500	5	50	0.4	245	0.0011
S <sub>10</sub>	500	10	60	1.6	229	0.0035
S <sub>11</sub>	500	15	30	3.0	179	0.0080
S <sub>12</sub>	500	20	40	2.6	214	0.0055
S <sub>13</sub>	550	5	60	1.9	226	0.0044
S <sub>14</sub>	550	10	50	0.6	237	0.0026
S <sub>15</sub>	550	15	40	2.9	193	0.0075
S <sub>16</sub>	550	20	30	3.1	184	0.0081

Sp No = Specimen No, A = Stirring speed (rpm), B = Stirring time (min), C = Stirring depth (mm), P = Porosity (%), US = Ultimate strength (MPa), WR = Wear rate (mm<sup>3</sup>/min)

The strengthening (tensile) test has been tested on a tensometer testing machine, JMI, Delhi by following ASTM E8 standard at room temperature. The shape of the tensile specimen is shaped in a dog-bone type. The dry-sliding wear tests have been investigated on the cylindrical specimen of Mg-hybrid composite by following the ASTM G99 standard.<sup>29</sup> The specimen dimensions of the wear test are 5 mm in diameter and 50 mm in length. The dry sliding wear test has been performed on pin-on-disc computerized tribometer, Workshop, DTU, Delhi with MS disc materials having a surface roughness of 1.5 Ra. The sliding speed and applied load during the tribometer test have been set as 5 m/s and 30 N, respectively. The constant sliding distance has been maintained at 1 km. Since the work was conducted on optimized processing parameters of stirring, the conditions of the wear experiment are to be fixed for all experiments. Before and after, the wear mass loss of Mg-composites has been measured by using an electronic weighing setup following ASTM G99 standards.

The output responses have been analyzed by using the mean values of the Main Effect Plots (MEP). Fig. 3 (a & c) calculate the rise of stirrer speed from the initial level (450 rpm) to the second position (500 rpm). This signifies the proper blending of AZ91Mg alloy and reinforcing particles yields low porosity and minimum wear rate in the fabrication of Mg-hybrid composite. However, when an increment in the stirring speed induced the penetration of gas in the

hybridized melt because of the initiation of pressure variation between the outer and inner surfaces of the compo-melt resulted in to increase in porosity and wear rate.<sup>30</sup> Also, the increment of stirring time leads to the evolution of oxides in the fabricated composite. This causes the declination of the tensile property i.e. ultimate strength of the Mg-hybrid composite. This can be examined from the evaluated mean effect data plots for the tensile strength of the Mg-hybrid composite as represented in Fig. 3(b).

**Results and Discussion**

**Microstructure and Porosity**

The metallographic studies of the fabricated Mg-composites have been studied using an electron microscope as shown in Fig. 4. The porosity of Mg-hybrid composites has been evaluated using the theoretical density calculated through Archimedes principle and compared with the base matrix as shown in Table 2 and Fig. 5.

Specimens S<sub>1</sub> and S<sub>16</sub> have noted that 4% increment in the porosity as illustrated in Fig. 4 (a & b) and Fig. 5. However, Fig. 4 (c–e) represents the metallographic images of specimens S<sub>6</sub>, S<sub>5</sub>, and S<sub>2</sub> respectively. As, these images show an increment in the pores of 3.6%, 3.7%, and 3.8% when compared to the base matrix. It is noted that specimens S<sub>8</sub> and S<sub>9</sub> represent only 1.5% of pores in comparison to the base matrix. The reduction in porosity can be validated from the micrographs as presented in Fig. 4 (f & g).

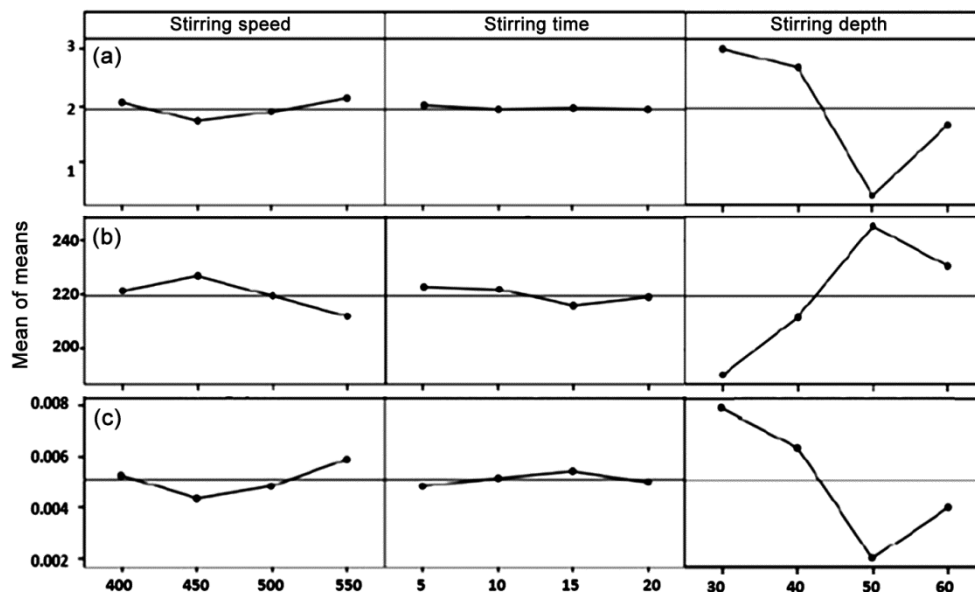


Fig. 3 — Mean main effect Plots for (a) Porosity, (b) Tensile strength, and (c) Loss of wear rate based on the parameters (i) Stirring speed (ii) Stirring time and (iii) stirring depth

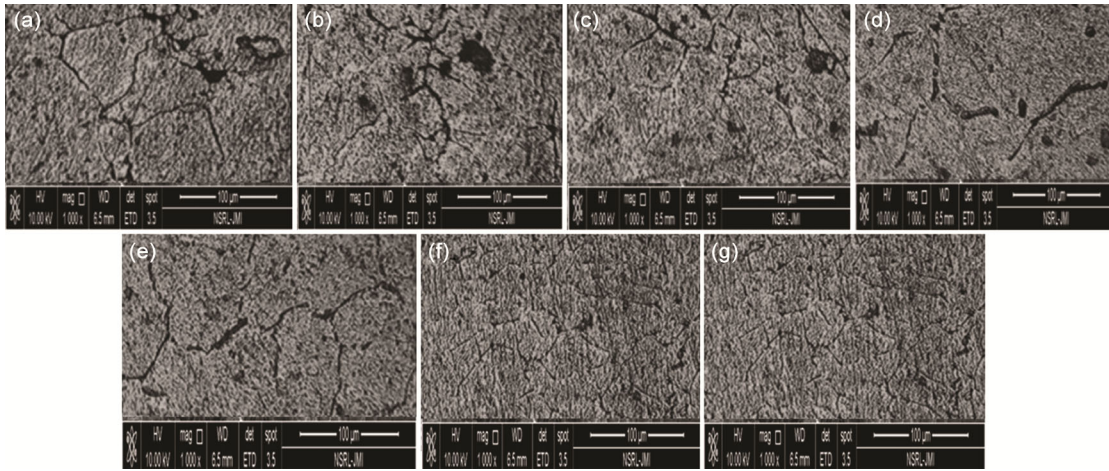


Fig. 4 — Microscopic Images of Mg-based composite specimens (a) S<sub>1</sub>, (b) S<sub>2</sub>, (c) S<sub>5</sub>, (d) S<sub>6</sub>, (e) S<sub>8</sub>, (f) S<sub>9</sub>, and (g) S<sub>16</sub>

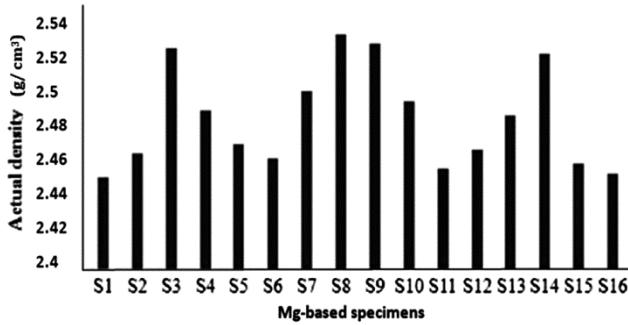


Fig. 5 — Comparison of actual density and fabricated Mg-composite specimens

**Desirable Functional Approach**

Different multi-objective optimization mechanisms are involved in various literature works like the study of grey relational technique, utility method, desirability approach, TOPSIS, etc. In the current research study, the desirability approach technique has been used for the optimization of multi-objective functions. As per this technique, the output responses of each desirability value after all the experimental runs have been evaluated and estimated by using two criteria i.e. (a) ‘larger is better’ or ‘nominal is better’ and (b) ‘smaller is better’.

In this research, porosity, and wear loss rate is considered as output parameters under the rule of ‘smaller is better’ whereas tensile strength has been analyzed with the rule of ‘larger is better’ criteria. The output response of the desirability value is fixed as ‘0’ if its values occur above the suitable range whereas the desirability value is fixed as ‘1’ if its data values are closer to the permissible range. Despite this, these acceptable ranges are determined as the upper and lower limits of the desirability output response values

from the experimentation. Specific desirability output response values have been calculated by using the given formula in Eqs. (1 & 2).<sup>(31)</sup>

$$d_i = \begin{cases} 1 & y_i \leq L_L \\ \left(\frac{U_L - y_i}{U_L - L_L}\right)^r & L_L \leq y_i \leq U_L \\ 0 & y_i \geq U_L \end{cases} \dots (1)$$

(‘Smaller is better’ criteria)

$$d_i = \begin{cases} 1 & U_L \leq y_i \\ \left(\frac{y_i - L_L}{U_L - L_L}\right)^r & L_L \leq y_i \leq U_L \\ 0 & L_L \geq y_i \end{cases} \dots (2)$$

(‘Larger is better’ criteria)

where,  $y_i$ : output (response) value,

$L_L$ : output lowermost (response) values,

$U_L$ : output uppermost (response) values and

$r$ : shape constant which represents the rank order of the estimated model of the output value (i.e. specific weight-age provided for output results)

In current work, each of the output outcomes is treated as equally significant, and thus ‘ $r$ ’ and ‘1’ values are considered for analysis. The desirability value of the Mg-hybrid composite (overall) is the key parameter that shows the combined effect of multi-output responses. Then by the virtue of another Eq. (3), the desirability values of Mg-hybrid composite ( $d_c$ ) for each experimental run are calculated.<sup>32</sup>

$$d_c = (d_1 \times d_2 \dots \dots \dots \times d_n)^{\frac{1}{n}} \dots (3)$$

where,  $d_1, d_2, \dots \dots \dots, d_n$  is the specific desirability output response of each value and  $n$  is the estimation of output results studied for this work.

The consolidation of measured input includes the highest absolute desirability value have been determined by the optimal solution. The assigned solution of measured inputs gives the optimal data values for each of the output (response) variables. The measured values of each desirability value of the Mg-hybrid composite are listed in Table 3. Based on the investigated results, the A3B1C3 combination has been determined as the fixed optimal factor. The evaluated values for ultimate strength, porosity, and wear loss rate are calculated as 245 MPa, 0.4%, and 0.0011 mm<sup>3</sup>/min respectively with the significant solution of each input parameter. The main effect plots include the SNR (signal-to-noise) ratio and mean ratio are equivalent to the overall desirable values evaluated by using Minitab 18 software and represented in Fig. 6(a & b). 0.5734 is the computed comprehensive mean output result value of all the Mg-hybrid composite desirable data values. Then, the layout of a regression design is formulated for the Mg-composite desirable value in contrast to the input values (A, B & C), with 0.9935 R<sup>2</sup> parameters as shown in Eq. (4).

Mg-hybrid composite desirability value  
 = -4.80674 + (0.014266 × A) + (0.42134 × B) + (0.048708 × C) - (5.45304 × 10<sup>-4</sup> × A × B) + (1.82485 × 10<sup>-6</sup> × A × C) - (9.5446 × 10<sup>-5</sup> × B × C) - (1.12412 × 10<sup>-5</sup> × A<sup>2</sup>) - (0.012407 × B<sup>2</sup>) - (6.73845 × 10<sup>-4</sup> × C<sup>2</sup>) ... (4)

Table 3 — Composite and individual desirable values of response values

Sp No	Individual desirability values				
	P	US	WR	CDV	Rank
S <sub>1</sub>	0	0.14	0.057	0	14
S <sub>2</sub>	0.16	0.43	0.257	0.265	11
S <sub>3</sub>	0.9	1	0.857	0.917	3
S <sub>4</sub>	0.46	0.67	0.585	0.569	7
S <sub>5</sub>	0.23	0.60	0.428	0.392	9
S <sub>6</sub>	0.13	0.32	0.157	0.189	12
S <sub>7</sub>	0.6	0.76	0.714	0.688	5
S <sub>8</sub>	1	0.87	0.971	0.946	2
S <sub>9</sub>	0.93	0.92	1	0.953	1
S <sub>10</sub>	0.53	0.70	0.642	0.622	6
S <sub>11</sub>	0.06	0	0.001	0	14
S <sub>12</sub>	0.2	0.50	0.342	0.326	10
S <sub>13</sub>	0.43	0.66	0.514	0.528	8
S <sub>14</sub>	0.86	0.81	0.771	0.817	4
S <sub>15</sub>	0.1	0.19	0.085	0.119	13
S <sub>16</sub>	0.03	0.07	0	0	14

Sp No = Specimen Number, P = Porosity ‘smaller is better’, US = Ultimate strength ‘larger is better’, WR = Wear rate ‘smaller is better’, CDV = Composite desirable values

The residuary data values for the derived regression designed formulation are conferred in Fig. 6. The residuary values represent each of the residual data outcomes shown within the range -0.02 and + 0.02 values, which confirms the adequacy of the regression formulation. The dual peaks of the histogram represent the homogeneous dispersion of the residual plots in contrast to the data results in Fig. 7.

**Validation test**

The validation test is executed empirically with the average Mg-composite desirable values to represent the divergence of all desirability values. The absolute sequence of the leading variable was obtained as (A4B3C2) which is ordered as 13 in desirability analysis and then in comparison with the optimal solution of input variables (A3B1C3). With the help of Eq. (5) confirmation test has been carried out.

**Predicted Mg-Composite Desirability**

Value =  $\gamma_m + \sum_{i=1}^l (\gamma_i^m - \gamma_m)$  ... (5)

where,  $\gamma_m$  are the absolute mean Mg-composite desirable values and  $\gamma_i^m$  is the average desirable data points at each independent solution.<sup>33</sup>

The actual and evaluated Mg-composite desirable values have been correlated and represents in Table 3. 0.834465664 is the calculated variation of the Mg-composite desirable values (optimal and initial

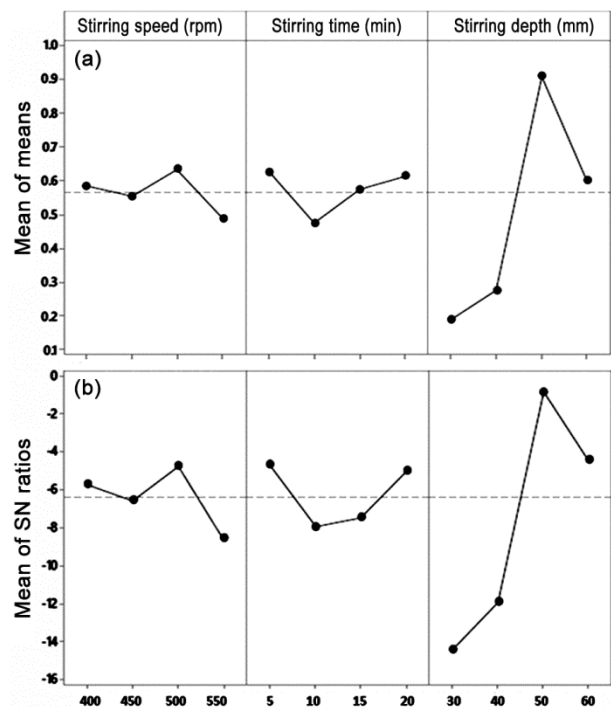


Fig. 6 — Mean main effect plots of (a) Composite desirable values (b) Signal to noise ratio of composite desirable values

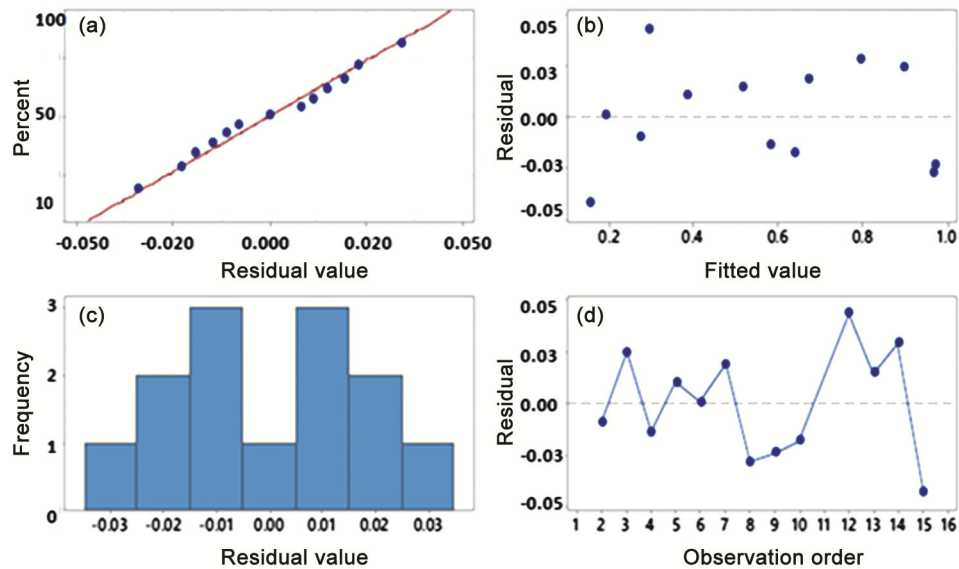


Fig. 7 — Plotting results of derived regression design formulation: (a) Normal probability plot, (b) Versus fits, (c) Histogram, (d) Versus order

Table 4 — Results of the validation test

Level	Optimal combination		
	Initial variable setting	Predicted	Direct approach base
Porosity (%)	A4 B3 C2	A3 B1 C3	
Ultimate strength (MPa)	1.8	0.4	
Wear Rate (mm <sup>3</sup> /min)	226	245	
Composite desirable values	0.0044	0.0011	
	0.119117115	1.0608	0.953763679

Table 5 — Analysis of Variance results

Input Parameters	DOF	SS	MS	F-Ratio	Contrib (%)
A, Stirring speed (rpm)	3	0.05530	0.018334	11.41	5.5387
B, Stirring time (min)	3	0.00304	0.001143	0.96	0.3432
C, Stirring depth (mm)	3	0.92989	0.309949	186.22	93.6260
Error	6	0.00449	0.001674		0.4921
Total	15	0.99272			100.00

DOF = Degree of freedom, SS = Sum of squares, MS = Mean of square, Contrib = Contribution

solution) by using the direct path. The concluded results in Table 4, it is observed that the evaluated value of optimal Mg-composite desirable value has been improvised in contrast with the selected prime set by 0.834465664. It is also found that porosity percentages for the significant solution are obtained as 2.8% and 1.3%. However, analogous tensile strengthening values are noted as 226 MPa and 245 MPa. Also, the wear rate data values are recorded to be 0.0044 mm<sup>3</sup>/min and 0.0011 mm<sup>3</sup>/min.

#### ANOVA

The influence of input factors for evaluating the optimum output outcome is investigated using ANOVA (analysis of variance) as shown in Table 5. It is noticed from the outcomes observed in Table 5 that the stirring

depth is found as the most significant input parameter/factor that leads to 93.272% of output responses. At similar time duration, the stirring time is found as the least affecting factor compared to other input factors considered.

#### Formation of Neural Network Structure

ANN is an effective modelling tool employed to identify the relation in-between the significant factors and the outcome results in different fields. The artificial networking method emulates the functions of the human intellect that includes the actions such as collecting the facts from the data, receiving the information, and evaluating the relation of the data variations.<sup>34</sup>

In this research work, a neural network is considered for the evaluation of the outcomes in-

between the input parameter ranges that are used in the experiments. By using MATLAB software, the ANN model of the current study is designed. The neuron-like points are showing in the input layers show the list of input factors like stirring time, stirring speed, and stirring depth. The neuron-like points in the output slab are similar to the 3 input parameters studied in this research, namely ultimate strength, porosity, and loss of wear rate. The dormant (hidden) slabs, linked through output and input layers, are boosted up in the ANN model to enhance the accuracy of the responses. One dormant slab is observed to be optimum subsequently performing the number of runs. The dormant layer comprises ten neuron-like points considered in the ANN model as represented in Fig. 8. The designed artificial network is competent and includes 80% of the accessible data and performed 20 percent of the left-out data by considering the back-propagation algorithm. 80% of the nourished input-out data sets (thirteen numbers), about 70% of competent data are considered for preparation and 15% of the data are values for confirmation as well as 15% of left-out data are employed for verification. The experimental outcomes of specimens S16, S9, and S1 are considered for the experiment of the artificial neural design, whereas all other data results are selected for the training scheme.

The regression ( $R^2$ ) responses for the experimenting and confirmed results as compared to actual outcomes are presented in Fig. 9 along with the correlation plot. These plots confirm the applicability of the derived artificial neural model. The results plotting of the derived artificial neural design is illustrated in Fig. 10. The neuron-like points approve the data accurately at zero periods (epoch) itself, and further focalize by operating the trials up to 1000 periods (epochs). After the experimentation of the neuron-like points, the derived network has been performed by using the experimental outcomes (i.e. S1, S9, and S16). However, this derived network helps to evaluate the competence of the design to investigate the required output results.

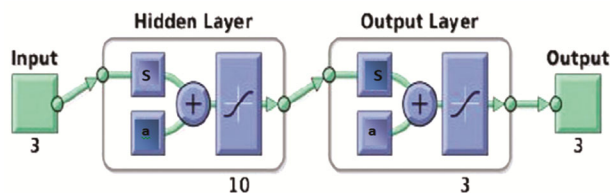


Fig. 8 — The Structure of modelled artificial neural network

**Affirmation of Artificial Predicting Model**

The estimated outcomes (Porosity, Tensile Strength, and Loss of Wear Rate) of considered experimental artificial neural design are correlated by using the actual experimenting data series and shown in Fig. 11(a–c). The relation data values represent a very minimal difference between the experimenting data series. It validates the suitability of the artificial neural design for the current study.

The microscopic images of the tensile test shows fracture in form of fine dimple flocks with tear ridges are represented in Fig. 12 (a & b). This represents the ductile failure of specimen S<sub>10</sub>. However, in S<sub>15</sub> showing coarse dimple flocks ridges confirms the ductile failure. Although, in a few places pores have been observed which act as the initiation of crack nucleation growth. Moreover, if this nucleation growth is successive then fails and considered as a tensile failure mechanism.

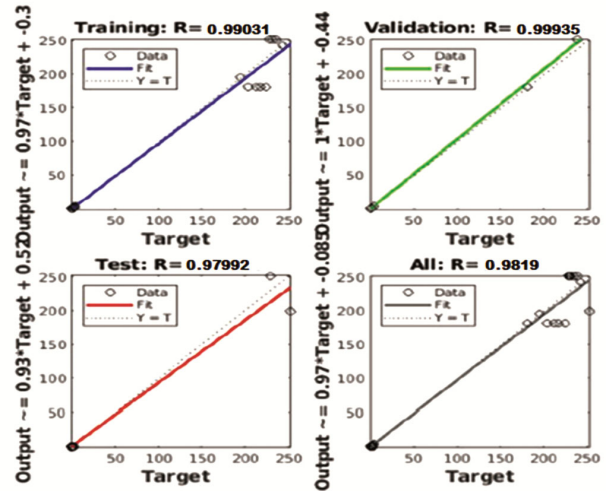


Fig. 9 — Correlation plots

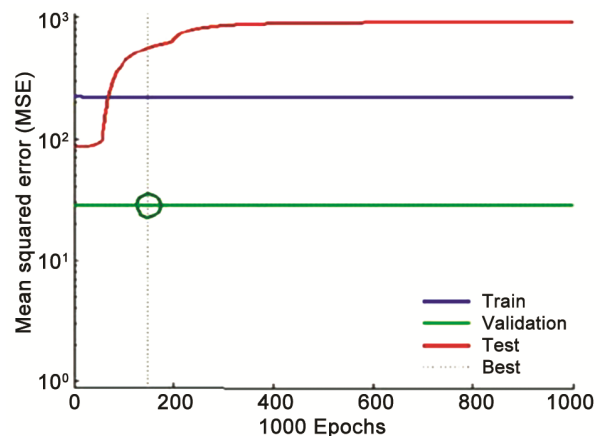


Fig. 10 — Performance curve of generated neural network (best validation performance is 28.1686 at epoch 148)

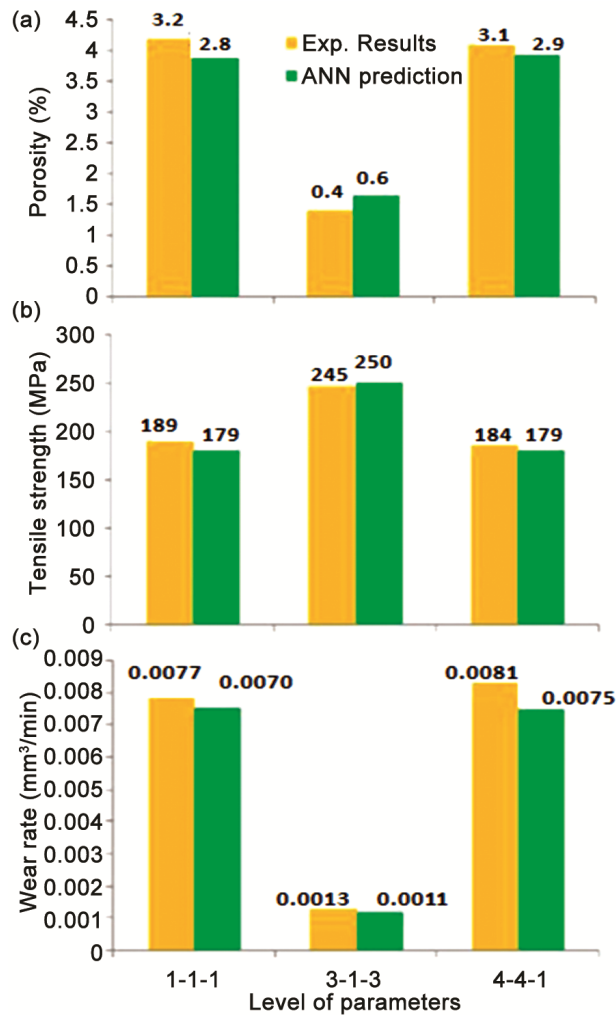


Fig. 11 — Compared results of experimenting and networking model of (a) Porosity, (b) Tensile strength and (c) Loss of wear rate

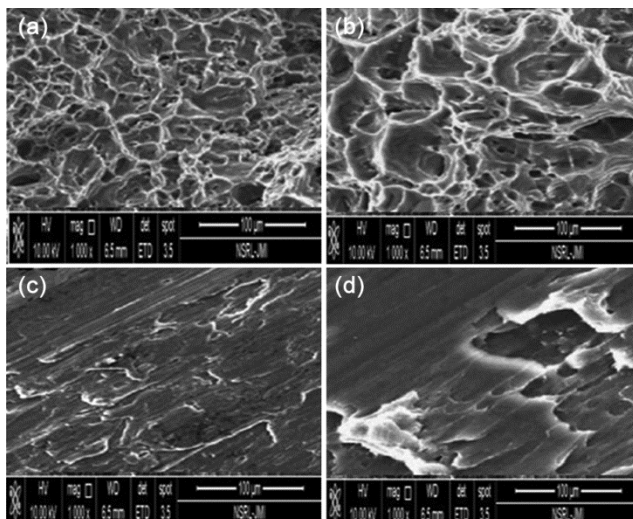


Fig. 12 — Microscopic image of tensile fracture (a & b) and Worn surfaces (c & d) of Mg-based S<sub>10</sub> and S<sub>15</sub> specimens

The microscopic images of the wear results of specimens S<sub>15</sub> and S<sub>10</sub> are represented in Fig. 12 (c & d). Both Mg-composites (S<sub>10</sub> & S<sub>15</sub>) show adhesive wear having white regions in form of oxide surfaces. The origin of oxidation behavior is because of the high interfacial temperature developed throughout the wear process.<sup>35</sup> In specimen S<sub>15</sub>, slight delamination of the surface has been observed. From mellow to severe wear transition region, adhesive wear and delamination have been observed which confirms the wearing of the Mg-composite specimens become stern.

### Conclusions

Hybrid AZ91Mg-composite has been successfully fabricated by using the vacuum-based squeezed stir cast process technique. The consecutive outcomes have been deduced that within the selected range of processing parameters and derived significant optimized results simulates high porosity and the formation of clusters in the hybrid composite melt. The stirring depth represents a uniform distribution of reinforcing particles in the Mg-hybrid composites. A non-linear regression design of Mg-hybrid composite propagates the desirable value i.e. R<sub>2</sub> data value of 0.9935 and confirms the validity test. However, ANN design develops the given series of experimental data values. The metallographic images of fracture surfaces of Mg-hybrid composite signify ductile fracture transition. The metallographic worn images of Mg-hybrid composite specimens show the delamination and adhesive behavior under different circumstances.

Thus these results give new divergence towards the designing of small-size surveillance airplanes parts such as ailerons, and wing flaps due to their suitability for abrasion wear of Mg-based composites under variable load and speed conditions. But during actual modelling analysis of such design parts, conditions may vary due to its validity as per requirements.

### Declaration

The authors confirm no possible conflict of interest regarding the authorship, investigation, and publishing of the current article.

### References

- Karaçor B & Özcanlı M, Investigation of the use of hybrid composite materials in automobile interiors, *Int J Automot Eng Technol*, **9(4)** (2020) 214–228, <https://doi.org/10.18245/ijaet.827239>
- Kumar P L, Lombardi A, Byczynski G, Murty S N, Murty B S & Bichler L, Recent advances in aluminium matrix

- composites reinforced with graphene-based nanomaterial: A critical review, *Prog Mater Sci*, (2022) 100948.
- 3 Prasanna S M, Yogesha K B, Mruthunjaya M, Shivakumar B P, Siddappa P N & Raju B R, Mechanical and tribological characterization of hybrid composites: A review, *Mater Today Proc*, **22** (2020) 2351–2358.
  - 4 Eacherath S & Murugesan S, Synthesis and characterization of magnesium-based hybrid composites—A review, *Int J Mater Res*, **109(7)** (2018) 661–672.
  - 5 Garg P, Jamwal A, Kumar D, Sadasivuni K K, Hussain C M & Gupta P, Advance research progresses in aluminium matrix composites: Manufacturing & applications, *J Mater Res Technol*, **8(5)** (2019) 4924–4939.
  - 6 Wang W, Han P, Peng P, Zhang T, Liu Q, Yuan S N & Wang K S, Friction stir processing of magnesium alloys: A review, *Acta Metall Sin*, **33(1)** (2020) 43–57.
  - 7 Singh S & Chauhan N R, Influence of B<sub>4</sub>C on microstructural, mechanical and wear properties of Mg-based composite by two-step stir casting, *Indian J Eng Mater Sci*, **28(2)** (2021) 189–197.
  - 8 Singh S & Chauhan N R, Microstructural and hardness study of stir-casted AZ91D/B<sub>4</sub>C MMCs, *Int J Microstruct Mater Prop*, **13(6)** (2018) 439–446.
  - 9 Singh S & Chauhan N R, Optimization of adhesive wear behavior of B4C/AZ91D-Mg composites, *Adv Mater Process Technol*, **8(4)** (2022) 4058–4072.
  - 10 Muhammad F & Jalal S, A comparative study of the impact of the stirrer design in the stir casting route to produce metal matrix composites, *Adv Mater Sci Eng*, (2021) 1–15, <https://doi.org/10.1155/2021/4311743>.
  - 11 Deepak J, Adarsha H, Bhat S & Kumar N R, Studies on development of alumina and ceria coated magnesium AZ91 composite for enhanced properties, *Mater Today Proc*, **46** (2021) 9027–9031.
  - 12 Singh N & Belokar R M, Tribological behavior of aluminum and magnesium-based hybrid metal matrix composites: A state-of-art review, *Mater Today Proc*, **44** (2021) 460–466.
  - 13 Kumar D & Thakur L, A Study of development and sliding wear behavior of AZ91D/Al<sub>2</sub>O<sub>3</sub> composites fabricated by ultrasonic-assisted stir casting, *Arab J Sci Eng*, **48** (2023) 2951–2967, <https://doi.org/10.1007/s13369-022-07032-9>.
  - 14 Srinivasan R, Jacob V, Muniappan A, Madhu S & Sreenevasulu M, Modeling of surface roughness in abrasive water jet machining of AZ91 magnesium alloy using fuzzy logic and regression analysis, *Mater Today Proc*, **22** (2020) 1059–1064.
  - 15 Kartheesan S, Khan B, Kamaraj M, Tekumalla S & Gupta M, Dry sliding wear behavior of magnesium nano-composites using response surface methodology, *J Tribol*, **144(1)** (2022) 011704, <https://doi.org/10.1115/1.4051410>.
  - 16 Krishnan M N, Suresh S, Vettivel S C, Prema C E, Arun J & Thirunamakodi P, Image texture description, surface-grains structure morphology, and prediction of wear parameters for Mg/B<sub>4</sub>C composites using response surface methodology, *Met Mater Int*, **28** (2022) 1195–1214, <https://doi.org/10.1007/s12540-021-01042-2>.
  - 17 Ravindran P, Mohamed M J S, Gnanaraj S J P & Appadurai M, Effect of graphite addition on dry sliding wear behavior of Self-lubricating Al-SiC-Gr hybrid composites by PM process, *Mater Today Proc*, **60** (2021) 783–787.
  - 18 Aydin F, Sun Y & Emre Turan M, Influence of TiC content on mechanical, wear, and corrosion properties of hot-pressed AZ91/TiC composites, *J Compos Mater*, **54(2)** (2020) 141–152, doi:10.1177/0021998319860570.
  - 19 Jeyaprakasam S, Kathirselvam M, Velmurugan C & Venkatachalam R, Experimental study of process parameters on machining performance in electro-discharge machining of 6061Al/TiC/Gr composites, *Surf Rew Lett*, **29(04)** (2022) 2250049, doi: 10.1142/S0218625X22500494.
  - 20 Prasad B K, Rathod S, Modi O P, Gupta G K & Yadav M S, Two-body abrasive wear behaviour of in-situ Al-TiC particle composites: Influence of TiC reinforcement and content in the alloy matrix and experimental parameters, *Tribologia-Finnish J Tribol*, **36** (2019) 4–23, <https://doi.org/10.30678/fjt.74449>
  - 21 Dash D, Samanta S & Rai R N, Flexural, dry sliding wear and machinability (EDM) characteristics of AZ91D/TiC (0, 5, 10, 15, & 20 wt%) MMCs, *Adv Mater Process Technol*, (2021) 1–19.
  - 22 Rajmohan T, Vijayabhaskar S & Vijayan D, Multiple performance optimization in wear characteristics of Mg-SiC nano-composites using grey-fuzzy algorithm, *Silicon*, **12(5)** (2020) 1177–1186.
  - 23 Chaluvharaju B V, Afzal A, Vinnik D A, Kaladgi A R, Alamri S & Tirth V, Mechanical and corrosion studies of friction stir welded nano Al<sub>2</sub>O<sub>3</sub> reinforced Al-Mg matrix composites: RSM-ANN modelling approach, *Symmetry*, **13(4)** (2021) 537.
  - 24 Arif S, Alam M T, Ansari A H, Shaikh M B N & Siddiqui M A, Analysis of tribological behaviour of zirconia reinforced Al-SiC hybrid composites using statistical and artificial neural network technique, *Mater Res Express*, **5(5)** (2018) 056506.
  - 25 Niranjan C A, Srinivas S & Ramachandra M, Experimental investigations on depth of penetration and surface integrity in AZ91/Al<sub>2</sub>O<sub>3</sub> nano-composites cut by abrasive water jet, *The Int J Adv Manuf Tech*, **107(1)** (2020) 747–762.
  - 26 Madhu K S, Venkatesh C V, Sharath B N & Karthik S, Effect of boron carbide on wear resistance of graphite containing Al7029 based hybrid composites and its dry sliding wear characterization through experimental, response surface method and ANOVA, *Tribologia-Finnish J Tribol*, **38** (2021) 48–60.
  - 27 Anand G, Alagumurthi N, Elansezhian R, Palanikumar K & Venkateshwaran N, Investigation of drilling parameters on hybrid polymer composites using grey relational analysis, regression, fuzzy logic, and ANN models, *J Braz Soc Mech Sci Eng*, **40(4)** (2018) 1–20.
  - 28 Velmurugan G, Perumal A, Sekar S & Uthayakumar M, Physical and mechanical properties of various metal matrix composites: A review, *Mater Today Proc*, **50** (2022) 1022–1031.
  - 29 Zaid H M A, Abed A R N & Hasan H S, Improvement of mechanical properties of magnesium (Mg) matrix composites reinforced with nano alumina (Al<sub>2</sub>O<sub>3</sub>) particles, *IOP Conf Series: Mater Sci Eng*, **671(1)** (2020) 01216, DOI 10.1088/1757-899X/671/1/012162.
  - 30 Majzooobi G H, Rahmani K & Atrian A, Temperature effect on the mechanical and tribological characterization of Mg-SiC nano-composite fabricated by high rate compaction, *Mater Res Express*, **5(1)** (2018) 015046, DOI 10.1088/2053-1591/aaa4e5.
  - 31 Vijayabhaskar S & Rajmohan T, Experimental investigation and optimization of machining parameters in WEDM of

- nano-SiC particles reinforced magnesium matrix composites, *Silicon*, **11(4)** (2019) 1701–1716, <https://doi.org/10.1007/s12633-017-9676-0>.
- 32 Premnath A, Optimization of the process parameters on the mechanical and wear properties of Al-SiC nano-composites fabricated by friction stir processing using the desirability approach, *Silicon*, **12(3)** (2020) 665–675, <https://doi.org/10.1007/s12633-019-00178-6>.
- 33 Vahdati M & Moradi, Statistical analysis and optimization of the yield strength and hardness of surface composite Al7075/Al<sub>2</sub>O<sub>3</sub> produced by FSP via RSM and desirability approach, *Iranian J Mat Form*, **7(1)** (2020) 32–45.
- 34 Kavimani V, Prakash K S & Thankachan T, Multi-objective optimization in WEDM process of graphene–SiC-magnesium composite through hybrid techniques, *Measurement*, **145** (2019) 335–349.
- 35 Aydin F, Sun Y, Ahlatci H & Turen Y, Investigation of microstructure, mechanical and wear behavior of B 4 C particulate reinforced magnesium matrix composites by powder metallurgy, *Trans Indian Inst Met*, **71(4)** (2018) 873–882, <https://doi.org/10.1007/s12666-017-1219-2>.